ICFD11-EG-4099

THE EFFECT OF TIP END-BLADE GEOMETRY ON THE AXIAL FANS PERFORMANCE

S. A. BESKALES,   SAMIR S. AYAD,   M. G. HIGAZY   and   O. E. ABDELLATIF

Faculty of Engineering at Shoubra, Benha University

ABSTRACT

A numerical study is carried out to investigate the effect of the addition of winglet to the end of blade on the axial fan performance. Validation and assessment of the used computer program FLUENT 6.2, is carried out by comparing its result with previous researcher. Simulation is then carried out to analyze the flow pattern with and without a winglet attached to the fan blade. Velocity distribution produced numerically showed that the winglet suppresses the secondary flow at the tip gap. Pressure distributions also confirmed the winglet advantages. Calculated performance of the fan used showed general increase of the fan efficiency with 3.5% above those without winglet at the optimum efficiency point and with up to 6 % at off design point.
.

KEYWORDS

Axial fan performance, Blade tip, CFD, Endplate, Simulation, Winglet, Tip leakage flow.

1. INTRODUCTION

Fans demand minimum gaps in order to facilitate operation, this gap tip clearance flow is known to have detrimental effects on the axial fans performance. The static pressure difference between the suction and the pressure side of the impeller blades produces a secondary flow over the tip of the rotor-blade as shown in figure 1. There is an interest in both the academic and industrial communities to minimize the negative effects of tip gaps. Ali and Cengiz [1] conducted experimental and computational analysis for various tip clearances to understand the effect of the tip leakage flow on aerodynamic performance of ducted fans, results showed that by decreasing the tip clearance from 3.04 % to 1.71 % increased the efficiency by 17.85 % at higher rotor speeds. Corsini et al. [2] conducted experimental and computational

investigations on a family of axial fans with special blade tip geometries to establish the aerodynamic merits of the proposed blade tip design concept. Blade tip end-plates were on the pressure side and the results showed that there was an improvement of rotor efficiency correlated to the control of tip leakage flow. Ali and Cengiz [3] used five different tip geometries also on the pressure side on the fan blade. The results showed that there was a significant gain in the axial mean velocity component. Reducing the tip clearance produced a considerable improvement of the fan efficiency. Michael [4] used a conic winglet at the tip blade and the results showed that the maximum gain in dimensionless volume flux is 4% near the free blowing region. Jeppe and Niels [5] investigated numerically the aerodynamics around a wind turbine rotor with winglets using CFD. Results showed that by adding a winglet to an existing wind turbine rotor increased produced power. Kokturk [6] studied the design and performance analysis of reversible axial ventilation fans using CFD tools, the results are embedded into the developed design procedure. The present work is concentrated on a commercially available axial fan with a winglet for both pressure and suction sides of the blade of the fan by Rosenberg GmbH of Germany. Computations are carried out with and without the winglet.
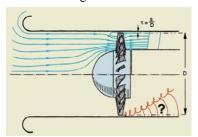

Figure 1 A Schematic flow diagram with generation of turbulence at the annular gap by difference in pressure [7].

2. COMPUTAIONAL TECHNIQUE
2.1 Governing Equations

In the cases where the experimental techniques for the problems are not appropriate to be applied, the engineers use the CFD tools to obtain information about the fluid flow problems and the flow parameters like pressure, velocity and temperature. Then he has to solve the basic equations to solve the phenomena, i.e. conservation equations of mass and momentum for pressure and velocity, energy equation for the temperature. The solution of these unknown variables needs an order to be followed, which the area of CFD plays its role.

The starting point of any numerical method is the mathematical model, [the set of partial differential equations and boundary conditions].

The continuity equation and the Navier-Stokes equations are needed to obtain the pressure and velocity around the flow field. For incompressible flow are as follows

Using tensor notation in Cartesian coordinates, continuity equation is:

$$\frac{\partial u_i}{\partial x_i} = S_m$$

S_m is source term and is set to [0] if there is no mass added to the continuous phase from dispersed second phase (e.g., due to vaporization of liquid droplets) or any source defined by the user.

Conservation of momentum (Navier-Stokes Equations) for incompressible flow is:

$$\rho \frac{\partial u_i}{\partial t} + \rho \frac{\partial (u_j u_i)}{\partial x_j} = -\frac{\partial p}{\partial x_i} + \frac{\partial}{\partial x_j}(2\mu s_{ij}) + \rho g_i + F_i$$

Where Fi is external body force and sij is the stress tensor which is given by:

$$s_{ij} = \frac{1}{2}(\frac{\partial u_i}{\partial x_j} + \frac{\partial u_j}{\partial x_i})$$

2.2 RNG (Renormalization Group) k-ε model

The RNG k-ε was derived using a rigorous statistical technique (called re-normalization group theory). It is similar to Standard k-ε model but includes following refinements:

- The RNG model has an additional term in its ε equation that significantly improves the accuracy for rapidly strained flows.
- The effect of swirl on turbulence is included in RNG model, enhancing accuracy for swirling flows.
- The RNG theory provides an analytical formula for turbulent Prandtl numbers while the standard k-ε model uses specified constant values.

- While the standard k- ε model is a high Reynolds number model, the RNG theory provides an analytically derived differential formula for effective viscosity that accounts for low Reynolds number effects.

These features make the RNG k-ε model more accurate and reliable for a wider class of flows than the standard k-ε model.

The transport equation for kinetic energy for RNG k-ε is as follows:

$$\frac{\partial k}{\partial t} + U_j \frac{\partial k}{\partial x_j} = G_k + G_b - \varepsilon + \frac{\partial}{\partial x_j}\left[\alpha_k \upsilon_{eff} \frac{\partial k}{\partial x_j}\right]$$

The transport equation for ε:

$$\frac{\partial \varepsilon}{\partial t} + U_i \frac{\partial \varepsilon}{\partial x_i} = \frac{\partial}{\partial x_j}\left[\alpha_\varepsilon \upsilon_{eff} \frac{\partial \varepsilon}{\partial x_j}\right] + C_{1\varepsilon}\frac{\varepsilon}{k}(G_k + C_{3\varepsilon}G_b) - C_{2\varepsilon}\frac{\varepsilon^2}{k} - R_\varepsilon$$

The model constants $C_{1\varepsilon}$ and $C_{2\varepsilon}$ have values derived analytically by RNG theory. $C_{1\varepsilon}$=1.42 $C_{2\varepsilon}$=1.68

G_k is the generation of turbulent kinetic energy due to mean velocity gradients and is defined as $G_k = \upsilon_T S^2$

Where S is the modulus of mean rate of strain tensor and is defined as $|s_{ij}| = \sqrt{2 s_{ij} s_{ij}}$

Gb is the generation of turbulence kinetic energy due to buoyancy and is given by $G_b = \beta g_i \frac{\upsilon_T}{pr_t}\frac{\partial T}{\partial xi}$

v_{eff} is the effective viscosity and is given by

$$d\left[\frac{\rho^2 k}{\sqrt{\varepsilon \mu}}\right] = 1.72 \frac{\bar{\upsilon}}{\sqrt{\bar{\upsilon}^3 - 1 + C_v}} d\bar{\upsilon}$$

Where $\bar{\upsilon} = \frac{\upsilon_{ff}}{\upsilon}$ $C_v \approx 100$

The above equation is integrated to obtain an accurate description of how the effective turbulent transport varies with the effective Reynolds number, allowing the model to better handle low Reynolds number and near wall flows.
In high Reynolds number limit

$$\upsilon_T = C_\mu \frac{k^2}{\varepsilon}$$

With Cμ=0.0845, derived using RNG theory.

2.3 CFD PROGRAM VALIDATION

Validation of the used computer program, FLUENT 6.2,[8] are carried out on a reversible axial fan. Present results are compared with the results produced by Kokturk [6].The design parameters and settings are presented for the reversible axial fan in table 1 and figure 2.

Table 1 Design summary, Kokturk [6].

	Hub	Mean	Tip
Radius (m)	0.41	0.71	1.01
Chord (cm)	36.4	31.9	18.2

Figure 2 Blade profiles at radial positions [6]

Figures 3 and 4 show the comparisons of the efficiency and total pressure. It is clear that there is an excellent quantitative agreement between the results by Kokturk [6] and the present work. The comparisons serve as good verification of the used program and it is possible to predict flow field using CFD tools.

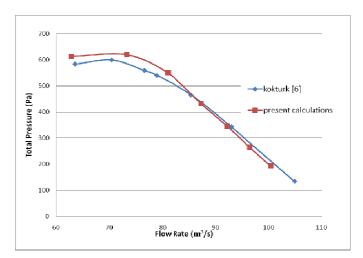**Figure 3 Performance efficiency curves for the Fan at N=1000 RPM.**

Figure 4 Pressure curves for the Fan at N=1000 RPM.

Figures 5 (a), (b), (c) and (d) show good general qualitative agreement between the present pressure contours and those produced by Kokturk [6].
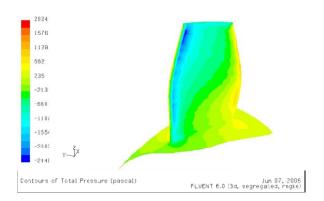

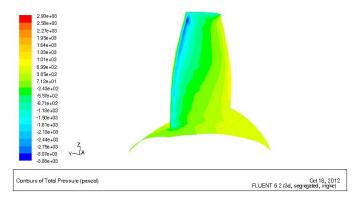**Figure 5 (a) Suction side of the blade, Kokturk [6].**

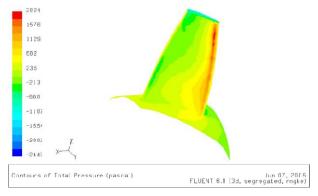**Figure 5 (b) Suction side of the blade, present work.**

3

Contours of Total Pressure (pascal)   Jun 07, 2005
FLUENT 6.0 (3d, segregated, rngke)

Figure 5 (c) Displays the pressure side, Kokturk [6].

Contours of Total Pressure (pascal)   Oct 18, 2012
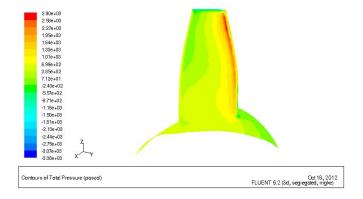FLUENT 6.2 (3d, segregated, rngke)

Figure 5 (d) Displays the pressure side, present validation.

3. PRESENT COMPUTATIONS

The CFD analysis of the axial fan is performed by the FLUENT commercial software version 6.2. The geometry and the computational grid are constructed with GAMBIT software version 2.2.30. Gambit is the pre-processor software used for preparing input data for CFD programs. It has also an add-on package namely G/Turbo, which is specifically designed for modeling turbo-machinery applications. This package provides automated geometry and meshing operations for blade row models. The model geometry can either be imported from an external program or generated within G/Turbo by the specification of curves describing the blade profile, hub edge and casing edge as shown in figure 6 for datum blade and figure 7 for blade with winglet. For full details of the blade geometry see reference [9].

The automated G/turbo option in gambit program couldn't build such these complicated details of winglet, and that is lead to manually subtract the winglet volume from the blade region and then assign the turbo zone and meshing the domain. Figure 8 shows the fan blade volume with winglet.
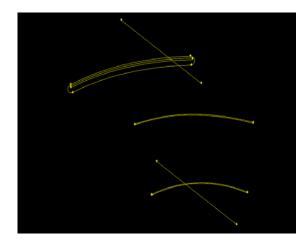
Figure 6 Datum blade profile in Gambit.

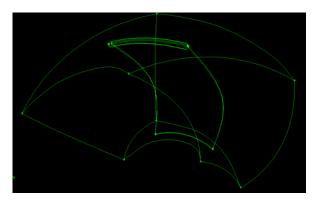**Figure 7 Blade profile with winglet in Gambit.**

Figure 8 Fan blade volume with winglet in Gambit.

4   Copyright © 2013 by ICFD11

3.1 Computational Mesh

The mesh is composed of triangular prisms and tetrahedral elements. There are approximately 258247 cell elements and 49469 nodes in the solution domain for datum blade and 249731 cell elements and 48167 nodes in the blade with winglet . Because the domain repeats itself in every blade, the entire domain is not modeled for the required solution, only the volume around one blade is meshed. Figure 9 shows the computational mesh of the solution of the datum blade [without winglet] and figure 10 shows the Computational mesh of the solution domain with winglet. In the figures, the interior elements are not shown to have the full visibility of the blade.
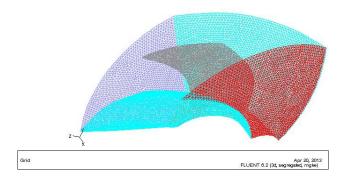

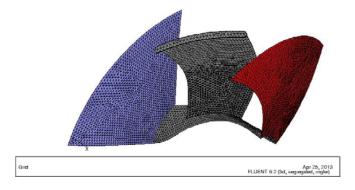**Figure 9 Computational mesh of the solution domain of datum fan.**

Figure 10 Computational mesh of the solution domain with winglet.

3.2 Boundary Conditions

There are two options to find the solution to the problem in FLUENT program. The first option is to define the inlet end exit of the turbo volume as pressure inlet and outlet type boundary conditions, respectively. The total gauge pressure at the inlet is entered by the user and the static gauge pressure at the exit is entered. After the solution is converged a volumetric flow rate and corresponding static or total pressure rise is calculated from the surface integrals or from Turbo option in fluent panel.

The second option is to define a velocity inlet boundary condition at the inlet section and pressure outlet at the exit. After a steady state solution is obtained, the pressure difference is calculated by using turbo options of the fluent program.
In the current analysis the inlet boundary is the pressure inlet and is taken to be zero and the outlet boundary in pressure outlet.

3.3 Solution Controls

The results are obtained with the solution of the continuity, N-S equations along with the equations for the selected turbulence model. In this present study, RNG [Renormalization Group] k- ε model is selected as the turbulence model.

After the boundary conditions are specified and the solution models are selected, the iterations are performed in FLUENT. The required number of iterations is determined by setting convergence criteria for the residuals for the three components of velocities, the continuity equation and the variable for the turbulence model [k and ε]. In most cases, the convergence criterion is set such that the difference between two successive iterations [residuals] is five orders of magnitude lower than the initial value.

The solutions for the datum blade are obtained with this criterion. During the solutions, iteration history is also checked for the stability and the trend of the residual curves. Figure 11 shows a typical convergence history graph of the solutions obtained for the datum blade. It is seen from the figure that the residuals for the variables are decreased to at least five orders of magnitude and a stable trend is reached at the end. The convergence histories of other solution variables like mass flow rate at outlet are also monitored to decide whether a reasonable solution is reached or not. Figure 12 shows the Convergence history graph for mass flow rate at 1000 RPM, ΔP = 67.5 Pa.

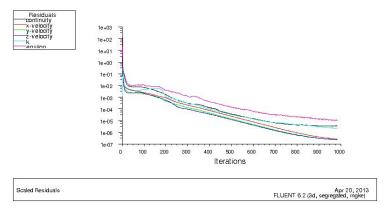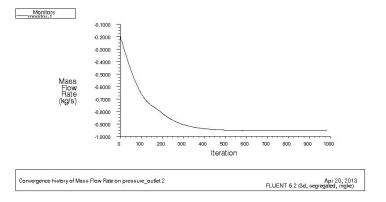**Figure 11 Convergence history graph**

Figure 12 Convergence history graph for mass flow rate at [RPM =1000, ΔP=67.5 Pa]

4. CFD RESULTS

4.1 Datum Fan

4.1.1 Pressure contours

The total pressure contours on the blades are given in figures 13. Figure 13 (a) shows the pressure side of the blade and figure 13 (b) displays the suction side. Dimensional values of pressures in Pa are given on the left scale of each figure.

The figures show a pressure difference of about 97 [Pa] between both sides at midpoint of blade tip at flow rate equal to 16759.4 [m³/h]
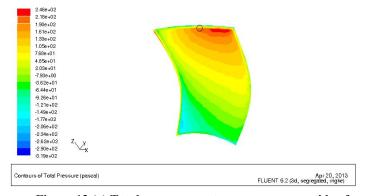

Figure 13 (a) Total pressure contours on pressure side of the datum blade.
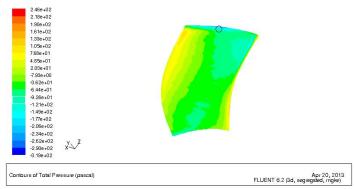

Figure 13 (b) Total pressure contours on suction side of the datum blade.

4.1.2 Velocity Contour

In order to have a better understanding of the velocity vectors and flow at the tip clearance region, three sections are considered as shown in figure 14.
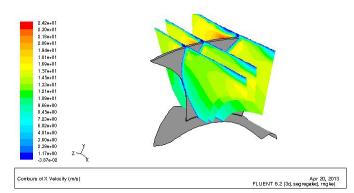

Figure 14 Contours of X direction velocity in all planes.

Figure 15 shows a considerable region of almost zero velocity in X-direction planes can be identified and even some flow reversible [leakage losses] at the datum blade tip which is the main reason for the secondary flow. This Secondary flow has a detrimental effect on the fan performance.
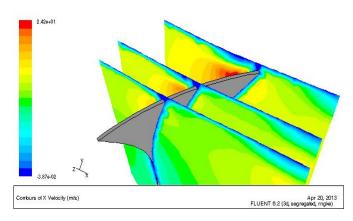

Figure 15 A close view of contours of X direction velocity in all planes.

6   Copyright © 2013 by ICFD11

4.2 Fan with Winglet

4.2.1 Pressure Contours

Figures 16 show pressure contours at flow rate equal 16977 [m³/h]. They show a pressure difference about 55 [Pa] between both sides at midpoint of blade tip which is considerably lower than that took place for the datum fan with same flow rate [see figure 13]
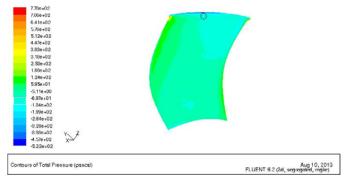

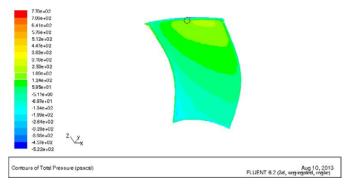**Figure 16 (a) Total pressure contours on the suction side of the blade with winglet.**

Figure 16 (b) Total pressure contours on the pressure side of the blade with winglet.

4.2.2 Velocity Contours

In order to have a better understanding of the flow, three sections are introduced at the x direction planes to capture the flow around the tip region as shown in figure 17.Figures 17and 18 indicate the effect of the winglet which is placed at the outer end of fan blade. The winglet acts as a barrier, which substantially blocks leakage around the blade tip. It is clear that there is an increase of X velocity component as compared with the case of datum fan shown in figure 15. The winglet reduces the vortices created in conventional fans by the reduction of differential pressure between the pressure side and suction side of the tip of the blade.

Velocity distribution produced numerically showed that the winglet suppresses the secondary flow at the tip gap.
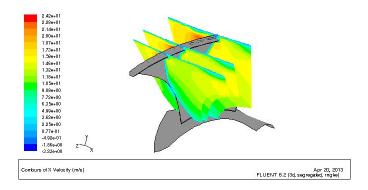

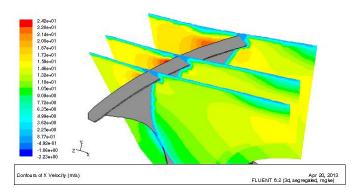**Figure 17 Contours of X direction velocity in all planes.**

Figure 18 A close view of contours of X direction velocity in all planes

4.2.3 The Effect of Winglet on the Axial Fan Performance

The iterations for the performance points for the axial fan with and without winglet are made by assigning different gage pressure values at the exit boundary of the domain, resulting in corresponding flow rates for the pressure differentials across the fan. The inlet pressures are kept constant. At the end the overall solution and the performance curve for the fan are given. The iterations are performed for the rotational speed of 1000 rpm.

Table 2 Comparison of computed performance points for the axial fan with and without the winglet 1000 RPM

Axial fan with winglet				
Flow-Rate m³/h	Total pressure pa	Efficiency %	Pressure coefficient ψ	Flow coefficient φ
13545.6	155.3	86.6	0.028	0.139
14479.3	135.3	87.3	0.024	0.150
15605.1	109.8	87	0.019	0.162
16977	72.7	79.7	0.012	0.178
18260.1	41.7	69.6	0.007	0.191
Axial fan without winglet				
13146.5	152	85.2	0.029	0.144
14160.6	130.9	86.3	0.025	0.154
15308.3	104.7	86	0.020	0.166
16759.4	67.5	79.7	0.013	0.180
18040.3	35.9	65.7	0.008	0.194

The data on table 2 are expressed graphically by the fan performance curves shown in figures 19 and 20 for 1000 RPM. They show that there is an enhancement of the axial fan performance curve after adding the winglet to the blade. This Improvement of rotor efficiency was correlated to the control of tip leakage flow by increasing the axial velocity near the tip region.

At the point of maximum efficiency [flow rate coefficient ⌀=0.165], the winglet caused an increase of efficiency of 3.5% above those without winglet.

The winglet gives even more pronounced improvement at off design points of operation. An example at ⌀ = 0.19 the winglet causes an efficiency increase of about 6 %.
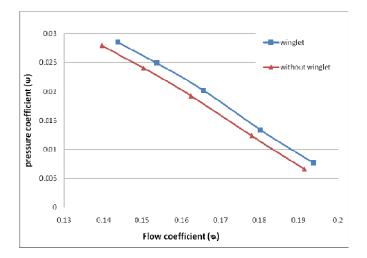
Figure 19 Dimensionless performance curves comparison between axial fan with and without the winglet at 1000 rpm.
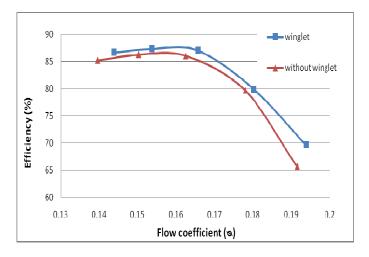
Figure 20 Efficiencies Comparison between axial fan with and without the winglet at 1000 rpm.

5. CONCLUSIONS

A CFD code is used to assess the effect of the winglet at the tip of the fan blade. The code is verified by comparisons of the present results with other researcher Kokturk [6]. A general good agreement between them indicated the soundness CFD code used. FLUENT program used to simulate the flow around the fan blade. Velocity vector, pressure contours and fan performance are presented.

The results show the following conclusions:

- The flow patterns on the axial planes show that a negative velocity always exists near the tip gap without the winglet while winglet exhibits a significant reduction in the leakage flow.

- Significant gains in axial mean velocity component are observed when a winglet extension is used.

- The winglet reduces the vortices created in axial fans by the reduction of differential pressure between the pressure side and suction side of the tip of the blade.

- The Numerical results demonstrate that the axial fan with winglets has the best fan performance. Results show that adding a winglet to existing fan blade increases efficiency around 3.5 % above those without winglet at the optimum efficiency point and with up to 6 % at off design point.

NOMENCLATURE

D: diameter [m]
k: turbulence kinetic energy [m²/s²]
N: rotational speed [rpm]
p: pressure [Pa]
Q: volumetric flow rate [m³/s]
η: hydraulic efficiency -
ρ: density [kg/m³]
ε: dissipation rate of turbulent kinetic energy [m²/s³]
Ψ: pressure coefficient = $\frac{P}{\rho \omega^2 D^2}$ -
⌀: flow coefficient = $\frac{Q}{\omega D^3}$ -
β: thermal expansion coefficient. [/°C]
μ: dynamic viscosity [Pa.s]
$C_{1\varepsilon}, C_{2\varepsilon}, C_{3\varepsilon}, C_v, C_\mu$: model constants
F_i: external body force. [N]
g_i: gravity acceleration [m/s²]
G_k: generation of turbulent kinetic energy
G_b:generation of turbulence kinetic energy due to buoyancy
pr_t: turbulent prandtl number
R_ε: additional term in ε equation
s_{ij}: strain rate tensor [s-1]
S_m: source term
u_i: instantaneous velocity component [m/s]

U_i: mean velocity component   [m/s]

α_ε, α_k: inverse effective prandtl number

v_{eff}: effective viscosity   [m²/s]

v_T: kinematic eddy viscosity   [m²/s]

ABBREVIATIONS

CFD: Computational Fluid Dynamic

RNG: Renormalization Group

ACKNOWLEDGMENTS

REFERENCES

[1] Ali, A., and Cengiz, C., "Tip clearance investigation of a ducted fan used in vtol uavs" ASME Turbo Expo, Vancouver, Canada, Vol. 7, 2011.

[2] Corsini, A., Rispoli, F., and Sheard, A.G., "Development of improved blade tip endplate concepts for low-noise operation in industrial fans", Journal of Power and Energy, Vol. 221, PP. 669–681, 2007

[3] Ali, A., and Cengiz, C., "Axial flow fan tip leakage flow control using tip platform extensions", Journal of Fluids Engineering, Vol. 132, No. 5, PP. 1–10, 2010.

[4] Michael, S., "Aeroacoustic optimization for axial fan with the lattice-boltzmann method", ASME Turbo Expo, Turbine Technical Conference and Exposition, Denmark, 2012.

[5] Jeppe, J., and Niels, N., " Numerical analysis of winglets on wind turbine blades using CFD", Wind Energy Department, Riso National Laboratory, Technical University of Denmark , Dept. of Civil Engineering, Aalborg University, Denmark, Personal

[6] Kokturk, T., "Design and performance analysis of a reversible axial flow fan", M. S. Thesis, School of National and Applied Sciences, Middle East Technical University, Turkey 2005.

[7] F. Kameier, W. Neise, "Experimental study of tip clearance losses and noise in axial turbomachines and their reduction" Journal of Turbomachinery, Vol. 119, PP. 460–471, 1997.

[8] Fluent 6.0. Documentation, FLUENT INC.

[9] S. A. Beskales, Samir S. Ayad, M. G. Higazy, O. E. Abdellatif, "The effect of tip end-blade geometry on the axial fans performance" M. S. Thesis, Mechanical Engineering Department, Faculty of Engineering at Shoubra, Benha University, Egypt, 2013.
.